ARTICLES

Simple model of large scale structure formation

R. K. Schaefer and Q. Shafi
Bartol Research Institute, University of Delaware, Newark, Delaware 19716
(Received 14 October 1993)

We explore constraints on inflationary models employing data on large scale structure mainly from Cosmic Background Explorer (COBE) temperature anisotropies and Infrared Asronomy Satellite (IRAS) selected galaxy surveys, taking care not to apply linear perturbation theory to data in the nonlinear regime. In models where the tensor contribution to the COBE signal is negligible, we find the spectral index of density fluctuations n must exceed 0.82. Furthermore, in inflation models which generate tensor fluctuations, these must contribute less than 20% of the signal seen by COBE. The data favor cold plus hot dark matter models with n close to unity and $\Omega_{\rm HDM} \sim 0.20$–$0.35$. We present realistic grand unified theories, including supersymmetric versions, which produce inflation with these properties.

PACS number(s): 98.65.Dx, 12.10.Dm, 98.80.Cq

I. INTRODUCTION

The inflationary universe scenario [1] provides an attractive resolution of the well known "horizon," "flatness," and "causality" puzzles encountered in the standard big bang cosmology. This scenario is most easily realized within the framework of both ordinary and supersymmetric grand unified theories (GUT's). In the simplest realizations of inflation, the density fluctuations are Gaussian and close to the Harrison-Zeldovich form, and the background density equals the critical density ρ_c. Primordial nucleosynthesis implies that less than 10% of the background density is composed of baryons, and so the bulk of matter is "dark," presumably in the form of relic elementary particles.

Almost a decade ago it was pointed out by Shafi and Stecker [2] that two types of dark matter, cold and hot, would provide, within the inflationary context, an elegant way of understanding observations, which indicated a surprising amount of clustering on larger than galaxy scales. Since the cold component clusters only on smaller scales, and the hot component clusters only on larger scales, such a universe would have an enhanced large scale power. Examples of GUT's containing cold plus hot dark matter (C+HDM) were also presented. The implications of this picture for microwave background anisotropies were worked out in 1989 [3,4]. Mass functions [5], bulk streaming motions [3,4], cluster number densities and correlation functions, as well as "great attractors" were also found to be compatible [6,7] with data.

Recent data on large scale structure from a variety of sources, particularly Cosmic Background Explorer (COBE) and Infrared Astronomy Satellite (IRAS) selected galaxy surveys, provide additional strong support to this remarkably "simple" scenario for structure formation. The COBE group [8] found an anisotropy amplitude, which they characterized by an averaged quadrupole moment amplitude $\delta T/T = Q_{\rm rms\text{-}PS}/T = 6.2 \pm 1.5 \times 10^{-6}$. As we have emphasized [9], the earlier predictions [3,4] for C+HDM models (3/4 CDM, 1/4 HDM) with negligible baryonic matter content were $7.8 \times 10^{-6}/b_8$, while for CDM alone they were significantly smaller ($4.7 \times 10^{-6}/b$), where b_8 =(rms mass fluctuation on the scale $8h^{-1}$ Mpc)$^{-1}$. Including a 5% baryon density (implied by primordial nucleosynthesis) modifies these predictions to $8.2 \times 10^{-6}/b_8$ for this C+HDM mixture and $5.1 \times 10^{-6}/b_8$ for CDM. Observationally derived values of b_8 seem to fall in the range $1.3 < b_8 < 2.5$, meaning the COBE result was in remarkable agreement with C+HDM models. COBE also lent some weak support for the inflationary power spectrum; the data are consistent with the $P(k) \propto k^n$ spectrum with $n = 1.1 \pm 0.5$ [8]. Following the COBE result other pieces of evidence pointing to the C+HDM model were discovered: compatibility with early quasar formation [10,11], compatibility with galactic correlations and velocities [12–14], Automated Plate Machine (APM) correlations [14,15], quiet local Hubble flow [16], "cosmic mach number" [17], and counts in cells [18,19]. Thus, there seems no doubt that the C+HDM model is a candidate worthy of serious consideration.

While we know that the primordial density power spectrum $P(k) \propto k$ with C+HDM provides a good fit to the data, it has long been known that the inflationary scenario does not quite yield this simple form. In recent studies, these correction factors have been exploited to yield power spectra $P(k) \propto k^n$ with n significantly less than 1 as a means to repair the relative large and/or small scale problems of the pure CDM model. In this paper, one of our tasks will be to undertake a study of the range of allowed n. (Note that in this work we will only consider $n \lesssim 1$, although inflationary models where n exceeds unity can be constructed [20].) Since we do not precisely know the HDM fraction of the universe, we will explore the two-dimensional parameter space $n - \Omega_{\rm HDM}$, and examine the constraints imposed by the data.

We do this by comparing the model predictions with data from COBE, the power spectrum of IRAS galaxies,

and bulk velocities from the potential flow reconstruction algorithm (known as POTENT) analysis. We will also consider requirements for the early formation of quasars. After fitting the normalization and the bias factor for IRAS galaxies, we evaluate χ^2 as a function of the parameters n and $\Omega_{\rm HDM}$. We present the results as χ^2 contour plots in the $n - \Omega_{\rm HDM}$ plane. We also consider the possibility that some of the COBE signal was produced by the long-wavelength gravity waves generated during inflation.

Because of uncertainties in the simulation of structure formation in the nonlinear gravity regime, we will concentrate chiefly on structure, which is still described by linear perturbation theory (scales $> 20h^{-1}$ Mpc). This avoids the difficulties inherent in identifying galaxies and clusters and separating out complicated dynamic effects, e.g., the velocity bias of galaxies. Our main aim is to explore a large region of parameter space, and try to identify that part of it for which running more detailed computer simulations would make the most sense.

Finally, if we are to take seriously the whole picture of inflation and C+HDM, we need to identify plausible models of inflation, which are compatible with our analysis of the large scale data. Here we will consider only "realistic" models of inflation. By this, we mean models which go beyond the usual minimum requirements of inflation, i.e., sufficient inflation for solving the horizon and flatness problems as discussed in [1]. We also desire the inflating field to be a part of a larger theory, which contains the following elements: neutrinos with masses in the eV range; a cold dark matter candidate; a high-energy particle physics structure, which is compatible with low-energy physics and its hints about higher symmetries; and a successful baryogenesis following inflation. Without these elements we find the inflation model to be somewhat *ad hoc*.

The plan of the paper is as follows. In the next section, we will describe our testing of inflationary models with large scale structure data in the linear perturbation regime. This will turn out to strongly limit the power spectrum. In Sec. III we will consider some general constraints from data, which come from structure in the nonlinear regime. This will limit mainly the HDM fraction. In Sec. IV we consider models of inflation, which satisfy all of our requirements for realistic inflation models. In particular we present some new examples of chaotic inflation based on supersymmetric grand unification. We end with some general conclusions in Sec. V. We have attempted to make this paper somewhat self-contained for a more general audience.

II. CONSTRAINTS FROM LARGE SCALE STRUCTURE DATA IN THE LINEAR REGIME

In this section, we will describe data and our analysis of theoretical predictions for these observations, but first we will discuss a few general issues concerning the models and the testing strategy employed here.

First of all, the problem with drawing strong conclusions about any given model of structure formation is that there are so many parameters to vary that we have a multidimensional parameter space to explore. We will choose best guess values of three of them, the baryonic fraction $\Omega_{\rm baryon} = \rho_{\rm baryon}/\rho_c$, the cosmological constant Λ, and the Hubble constant, $H_0 = 100h$ km sec^{-1}, with h observationally constrained to the values $0.4 \lesssim h \lesssim 1.0$. Constraints on the age of the universe from globular star clusters, nuclear cosmochronology, and white dwarf ages imply that high values of the Hubble constant are forbidden, i.e., $h < 0.6$ in an $\Omega = 1$ universe. Thus these models will be allowed only if the observations eventually settle into a more restricted range $0.4 < h < 0.6$. Since many quantities vary as h^2 there is still some freedom despite this narrow range of Hubble constant. In the present analysis we will use only the central value, $h = 0.5$.

Primordial nucleosynthesis strongly constrains the baryon density [21] as $0.010 \leq \Omega_{\rm baryon} h^2 \leq 0.015$. Using $h = 0.5$, we can express this 95% confidence constraint as

$$\Omega_{\rm baryon} = 0.05 \pm 0.01 \ . \tag{2.1}$$

We note that allowing for the uncertainty in h, the baryonic fraction could range from $\Omega_{\rm baryon} \sim 0.03 - 0.09$. We intend to explore this uncertainty in the Hubble constant and baryon fraction and its implications in a future publication. Once we have fixed the baryon density, the other densities can be completely specified by the hot dark matter density $\Omega_{\rm HDM}$ as

$$\Omega_{\rm CDM} = 1 - \Omega_{\rm baryon} - \Omega_{\rm HDM}.$$

The hot dark matter fraction (combined with the Hubble constant) also specifies the neutrino mass. If we have one flavor of neutrino whose mass is in the eV range, usually taken to be ν_τ, then

$$\Omega_{\rm HDM} = \left(\frac{m_{\nu_\tau}}{23 \text{ eV}}\right)\left(\frac{0.5}{h}\right)^2 . \tag{2.2}$$

We will set the cosmological constant (Λ) to zero. There is evidence to support this choice. The local (within $60h^{-1}$ Mpc) velocity field implies values of Ω close to unity [22]. Furthermore, in a Λ-dominated universe, there seems to be too few gravitational lensing events [23], and the bulk streaming velocities are too small [18].

The growth of density fluctuations is affected by the dynamics of the matter content, producing a scale-dependent modification of the density-fluctuation power spectrum. The relative growth as a function of scale is discussed in Appendix A, and the results are summarized in Fig. 1, where we present the transfer functions in Fourier space as a function of Fourier wave number $k = 2\pi/\lambda$. In Fig. 1, we see that increasing the neutrino fraction decreases the amount of growth, and hence the amplitude, on small scales (large k). We also note that there are some modifications of the shape of the spectrum on quite large scales. For example the transfer function with $\Omega_{\rm HDM} = 0.3$ is slightly steeper at $k \sim 0.07h$ Mpc^{-1} than that of either $\Omega_{\rm HDM} = 0.0$ (CDM) or $\Omega_{\rm HDM} = 0.5$.

In order to do our comparison in the most unambigu-

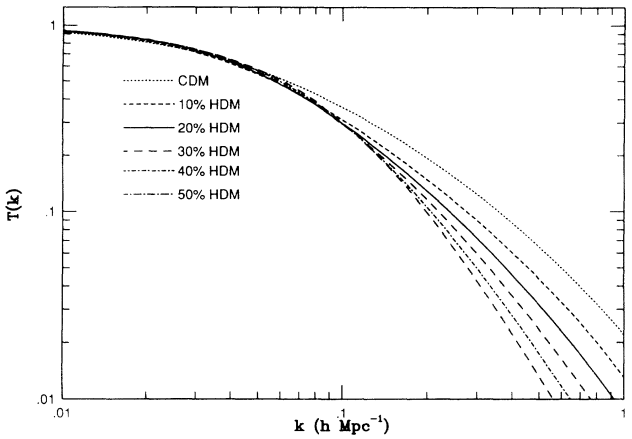

FIG. 1. Transfer functions for the cold plus hot dark matter models. The curves represent the relative growth of density fluctuations as a function of scale. The curves represent the present time (z=0) transfer functions and in a universe with $\Omega_{\rm CDM}+\Omega_{\rm HDM}+\Omega_{\rm baryon}=1$, where we have taken the canonical value of $\Omega_{\rm baryon}=0.05$ from primordial nucleosynthesis.

ous way, we will confine our attention mostly to the regime where linear theory is appropriate. In the past, it was common to normalize linear power spectra by use of the fact that the rms optically selected galaxy density fluctuations are $\delta N/N=1$ on a scale of 8 h^{-1} Mpc. In the most naive case, where one assumes that galaxies (light) trace the mass distribution, one would set the rms mass fluctuation also equal to one on this scale. More recently, however, it has become apparent that the galaxies are more strongly clustered than the mass, i.e., they are biased tracers of the mass. The usual method for dealing with this complication is to assume that there is a linear relation between the optical galactic density and mass fluctuations using a bias parameter b, which is independent of scale $b=(\delta N/N)/(\delta M/M)$. The mass fluctuation $\sigma(R)$ in a sphere of radius R is calculated in linear theory by

$$\sigma^2(R)\equiv\frac{1}{2\pi^2}\int_0^\infty dk\ k^2P_{\rm th}(k)\left[3\frac{j_1(kR)}{kR}\right]^2, \qquad (2.3)$$

where $j_1(x)$ is the first spherical Bessel function and the term in brackets is the Fourier transform of a sharp edged sphere of radius R. Clearly, when a perturbation amplitude approaches unity, linear theory is no longer appropriate. Even with b as large as 2, this implies $\sigma(8h^{-1}$ Mpc$)=0.5$, which is still quite nonlinear. Using the spherical collapse approximation (see Appendix B) we estimate that for $\sigma=0.5$, we are already highly contaminated by nonlinear effects. If we consider scales for which $\sigma(R)\leq 0.4$ we estimate that the nonlinear corrections will be $\lesssim$30%.

A look at Fig. 1 shows that the greatest difference between the models considered here occurs on the small scales. Limiting our range to $k\leq 0.3h$ Mpc^{-1} implies that our testing will have a somewhat weakened ability to discriminate between models with different HDM fractions. In Sec. III we will consider some constraints from nonlinear structures to help us pin down the dark matter fraction. We will first give a brief description of the large scale structure data, followed by a description of our calculations for different models.

A. Large-scale structure data

Here we will discuss the particulars of the data we are using. We explain our reasons for choosing the data and method of interpretation of this data.

1. COBE data

The large amplitude of the COBE measured temperature fluctuations is characterized by the extrapolated quadrupole moment $Q_{\rm rms\text{-}PS}$. This amplitude was a factor of 2–3 larger than predicted in the usual CDM models fit to galactic structure, and so gave strong support for the C+HDM models [9]. However, various authors do not seem content to use the COBE analysis of the amplitude. Instead they choose to use the sky variance at 10°, which, when used with a Gaussian beam, implies a somewhat smaller amplitude for the fluctuations (e.g., [15,24] corresponding to $Q_{\rm rms\text{-}PS}=15.3$ μK). The COBE beam pattern, however, is only approximately a Gaussian shape. More careful analysis of the COBE results [25] using the actual beam pattern seems to confirm the original higher value of the amplitude. In addition, use of the correct beam pattern reduces the variance of the fit amplitude, so the best fit $n=1$ COBE amplitude now corresponds to $Q_{\rm rms\text{-}PS}=17.4\pm3.1$ μK (extrapolated from the hexadecupole). Although it is customary to quote the results in terms of the quadrupole moment, this corresponds to only the very small wave number end of the spectrum. The best-fit amplitude of the quadrupole moment will be somewhat dependent on the value of n used in the analysis. In order to find a better quantity than the quadrupole, Wright *et al.* [25] recommend normalizing the amplitude to the hexadecupole $\delta T_4=12.8\pm2.3$ μK, when $n\neq 1$, as in the inflationary models we consider here. This yields a best fit amplitude less dependent on the value of n.

We note that the COBE results have been confirmed by a balloon experiment from the MIT/GSFC/Princeton Collaboration [26], which sees the same temperature correlation function as COBE and find similar values for the fluctuation amplitude, which they specify with $Q_{\rm rms\text{-}PS}$. However, they currently only have data from the northern hemisphere and their limits on $Q_{\rm rms\text{-}PS}$ are not as constraining as those for COBE. In the future they plan to cover the southern hemisphere as well, which would improve the limits of the COBE power spectrum exponent.

Ideally, we would like to include the detections of smaller scale anisotropy experiments in this analysis. There has been a wave of new detections of temperature anisotropies on $1^\circ-2^\circ$ scales. It is not clear that all of the detections are giving a totally consistent picture, and

even different scans with the same instrument give different results. A possible explanation is that the systematic errors these experiments face are quite complicated. We expect that these uncertainties will be resolved and that we will know the amount of degree scale anisotropy, which exists with some precision. We also point out that C+HDM models, when normalized to COBE produce the same degree scale anisotropies as similarly normalized CDM models. The only differences occur for anisotropy measurements $\ll 1°$. Since the degree scale anisotropies are all in the right ballpark for $\Omega = 1$, $n \approx 1$ models normalized to COBE, we take this as an encouraging sign for the models we consider in this paper.

2. *The IRAS large-scale survey of galaxies*

The IRAS survey of galaxies done by the QDOT (Queen Mary-Durham-Oxford-Toronto) Collaboration [27], extends as deep as several hundred Mpc, approaching the smallest scales observable by the COBE satellite. Combining the COBE data with the IRAS survey of galaxies thus covers the whole range of scales where the fluctuations can be described by the linear theory. The QDOT IRAS survey has measured redshifts for 1-in-6 IRAS galactic sources (1824 galaxies) with IRAS fluxes > 0.6 Jy. The IRAS selected galaxies seem to be more uniformly distributed than optically selected galaxies and may therefore give a fairer representation of the universe. By concentrating on measuring only 1-in-6 galaxies, the QDOT Collaboration obtained a deep sparse sample out to a depth larger than that of the Berkeley IRAS survey [28], which measured redshifts for all IRAS sources above a flux of 1.2 Jy. Using the redshift of the source as a distance indicator, combined with angular position data, one has a three-dimensional picture of the galaxy distribution. This distribution can be analyzed to directly extract the power spectrum of density fluctuations [28,29]. The results of the Feldman, Kaiser, Peacock [29] analysis is shown as the power spectrum data in Fig. 2.

We will use this QDOT IRAS data to test models with theoretical power spectra given by

$$P_{\rm th}(k) = Ak^n[T(k)]^2. \tag{2.4}$$

For $n \sim 1$ and the transfer functions $T(k)$ in Fig. 1, we can see that the power spectra go like $P(k) \sim k$ on very large scales and like $P(k) \sim k^{-3} - k^{-4}$ on very small scales, with a peak somewhere around $k \sim 0.02 - 0.10$. In order to get the proper normalization for the amount of structure on scales up to the power spectrum peak scale, one must measure the power on scales larger than the power spectrum peak scale. In the mass fluctuation integral [Eq. (2.3)] there are significant contributions to the mass fluctuations in 20 Mpc spheres coming from 100 Mpc scales ($k \sim 0.03h$ Mpc^{-1}). Thus we feel that to test power spectra of the type considered here, we require a survey out to a depth at least as large as the QDOT survey. A comparison of the QDOT and 1.2 Jy Berkeley power spectra, (see Ref. [29]), suggests that the Berkeley survey may still be too small to be seeing all of the large scale power.

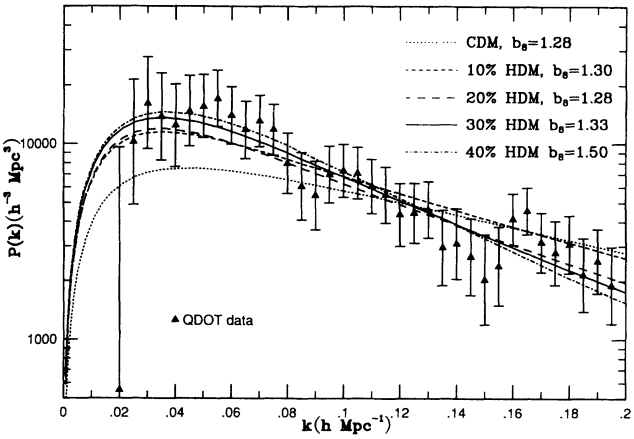

FIG. 2. We show the calculated model power spectra using our best fit model parameters for $n = 1.00$ only. The values of b_8 and b_I have been fit as described in the text. The values of b_I are close to 1.0, with the values $b_I = 1.1$, 1.1, 0.9, 0.9, and 1.0 for $\Omega_{\rm HDM} = 0.0$, 0.1, 0.2, 0.3, and 0.4, respectively.

3. *POTENT bulk flow velocities*

We also use the bulk flow velocities from the POTENT analysis [30]. They represent the the rms velocities of spherical regions of radius R. The velocity has first been filtered with a Gaussian of width $R = 12h^{-1}$ Mpc to reduce noise. This data is shown in Fig. 3. Unfortunately, the POTENT analysis suffers from the problem that not enough of the universe has been sampled to get a fair estimate of the average velocities. This is exacerbated by the fact that velocities are even more sensitive to the very large scale power than the mass fluctuation. However, we would still like to use these velocities because they do not depend on the bias. (Velocities are generated by the gravity of density fluctuations.) Since we have velocities from one local patch, we will include the cosmic variance of the predicted velocity for any given patch of the universe in our analysis. Our treatment will be described in the next section.

B. The χ^2 test of parameters

We are interested in the limits we can obtain on the paramters n and $\Omega_{\rm HDM}$. The procedure for doing this has been explained in detail in an article by Avni [31], so we will relate only a few salient features. To begin, we will call n and $\Omega_{\rm HDM}$ the "interesting parameters." In order to do the testing, we must fit two other parameters, the normalization and IRAS galaxy bias, which we call "uninteresting parameters." After fitting the uninteresting parameters for each value of n and $\Omega_{\rm HDM}$, we then sum the square of the differences between the predictions $y_i^{\rm th}$ and the observations $y_i^{\rm obs}$, weighted by the observational

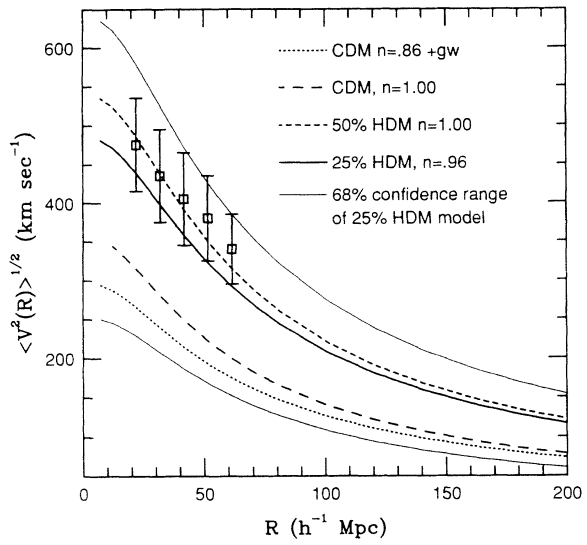

FIG. 3. The values of the bulk streaming velocities extracted by the POTENT analysis program with one σ error bars [29]. Also shown are predicted velocity curves for selected models. The models with low n and gravity waves can be ruled out by this data even though the cosmic variance for the velocity predictions in a single region are quite large. To illustrate this we have plotted the 68% confidence limits on the prediction of large scale streaming velocities for the 25% HDM model.

errors $\sigma_i^{\rm obs}$. We call this sum S

$$S(\Omega_{\rm HDM}, n) = \sum_{i=1}^{N} \left(\frac{y_i^{\rm th} - y^{\rm obs}}{\sigma_i^{\rm obs}} \right)^2 . \qquad (2.5)$$

There will be a minimum value of this sum $S_{\rm min}$ for some value of n and $\Omega_{\rm HDM}$. We then define a quantity ΔS

$$\Delta S(\Omega_{\rm HDM}, n) = S(\Omega_{\rm HDM}, n) - S_{\rm min}. \qquad (2.6)$$

ΔS then has a χ^2 probability distribution with 2 degrees of freedom (for the two interesting parameters).

The confidence levels for accepting or rejecting the models are then calculated using the $\chi^2(2)$ statistic. To understand the results of the testing procedure, we will make plots of our n-$\Omega_{\rm HDM}$ space, and then draw countours corresponding to $\chi^2(2)$ confidence levels of 25, 50, 68, 95, and 99 %. Models outside of the contours are ruled out with at least that degree of confidence.

We would like to be precise about the meaning of this test. Given that the free parameters are n and $\Omega_{\rm HDM}$, this test limits the range of these parameters. As we will show, it rules out $\Omega_{\rm HDM} = 0$ (all dark matter is CDM) models with >99% confidence for all values of n. However, if one believes *a priori* that $\Omega_{\rm HDM} = 0$, for example, then the test we have done will not give us the allowed range of n for a pure CDM model. For that information, one needs to redo the test using the $S_{\rm min}$ of the best-fit CDM model and calculate limits based on χ^2 with 1 degree of freedom (n). On the other hand, the fact that all CDM models will be excluded in our version of the test already informs us that models in which we allow $\Omega_{\rm HDM} \neq 0$ yield much improved fits to the data than any of the pure CDM models.

In our analysis we use the 36 values of the IRAS $P(k)$, the 5 POTENT velocity values, the b_I determination, and the COBE amplitude. The COBE amplitude has been independently confirmed by the far infrared survey (FIRS) balloon experiment [26]. Since so far their results are only presented as a confirmation of COBE, we will count the COBE result twice in our sum S: once for COBE itself, and again for the FIRS experiment. This forces the amplitude of density perturbations to be slightly closer to the COBE normalized amplitude than by weighting it as only one point. The results of the analysis is quite similar if we were to weight COBE as only one data point. Thus we have effectively a total of $N = 44$ data points, which contribute to S.

For each value of n and $\Omega_{\rm HDM}$ we must fit the uninteresting parameters, i.e., find the values of b_8 and b_I, which minimize $S(b_8, b_I)$ for each model. We will now proceed to discuss how we compute the $y_i^{\rm th}$.

C. Model predictions from linear theory

Here we will explain how we compare our theoretical power spectra $P_{\rm th}(k)$ to the data presented in the preceding section. First of all, we can calculate the hexadecupole δT_4 (measured by COBE) with the formula given in Ref. [32] for the coefficient of the fourth spherical harmonic for each of the power spectra we are considering. However, we can find an effective wave number $k_{\rm eff}$ for which the amplitude of $P(k_{\rm eff})$ is directly proportional to the amplitude of the hexadecupole. We have found that the value $k_{\rm eff} = 1.05 \times 10^{-3} h$ Mpc^{-1} accurately characterizes the hexadecupole moment for the limited range of n we are studying ($0.80 < n < 1.00$).

The COBE experiment cannot distinguish between temperature fluctuations generated by the Sachs-Wolfe effect of scalar (density) fluctuations and tensor (gravity wave) fluctuations, both of which are products of inflation. This signal confusion is worsened by the fact that the ratio of the moments generated (at least on COBE scales) for scalar and tensor contributions are nearly independent of scale [33–35]. The overall amplitudes of the moments for scalar and tensor modes, however, can be quite different, and one must construct a specific model of inflation and then evaluate the density perturbation and gravity wave amplitudes during inflation. In some models of inflation, such as "new" inflation [1], the contribution of gravity waves to the COBE signal is negligible, and the COBE signal relates only to the scalar density perturbations.

Models of inflation, which produce a significant amount of gravity waves, cannot be summarized with a universal formula. However, there is a relation derived from the model "power-law inflation" [36], which relates the gravity wave (tensor) contribution to the COBE signal $(\Delta T/T)_T$ to the contribution from the density (scalar) fluctuations signal $(\Delta T/T)_S$ via the spectral exponent of the density power spectrum n [24,34,37]:

$$\frac{(\Delta T/T)_T^2}{(\Delta T/T)_S^2} \approx 7(1-n). \tag{2.7}$$

This relation also is reasonably accurate for chaotic inflation models. Since the COBE signal is a quadrature sum of the multipole moments, decreasing n decreases the fraction of COBE signal due to density waves, and thus implies a smaller amplitude for $P_{\rm th}(k)$. Thus the amplitude of the COBE quadrupole moment is $\sqrt{8-7n}$ times larger than would be expected from the density component alone. We will consider models with gravity waves produced according to this formula.

To simulate the IRAS power spectrum $P_I(k)$ we have to apply a couple of correction factors to our theoretical $P_{\rm th}(k)$. First of all the distribution of galaxies in redshift space on large scales appears more clustered because of the Doppler contribution to the redshift from velocity perturbations [38]. With a biased galaxy distribution (b_I) this correction can be made by multiplying with the factor

$$P(k) \to \left[1 + \frac{2}{3b_I} + \frac{1}{5b_I^2}\right] P(k)\ . \tag{2.8}$$

However, on smaller scales there is the opposite effect; the Doppler shifts from the peculiar velocities of galaxies become large in comparison to the Hubble velocities and in fact wash out this redshift clustering effect. This effect can be described with a velocity dependent factor [39]

$$P(k) \to P(k)\frac{\sqrt{\pi}}{2}\frac{\mathrm{erf}(kR_v)}{kR_v}\ , \tag{2.9}$$

where $R_v = 4.4\ h^{-1}$ Mpc for IRAS galaxies.

Applying these corrections to a linear power spectrum seems to give reasonable agreement with the power spectrum of "galaxies" in N-body simulations. For example, Feldman, Kaiser, and Peacock [29] present such a power spectrum (from Ref. [13]) for a model with 30% HDM. The N-body spectrum becomes slightly higher than our linear spectrum for $k \gtrsim 0.15$ presumably due to nonlinear corrections. The worst disagreement ($\lesssim$30 %), occurs at the small wavelength end $k = 0.2h$ Mpc^{-1} of the QDOT IRAS $P(k)$. This error is still much smaller than the QDOT error bars, so we believe our procedure is relatively insensitive to nonlinear effects.

To do the testing, we first must calculate the linear theory power spectra for all models with a primordial power spectral index $0.80 < n < 1.00$ and $0 < \Omega_\nu < 0.5$. We have limited n to be ≤ 1 because we are considering only grand unified models of "new" and "chaotic" inflation. We calculate the power spectra for these models in steps of $\delta n = 0.02$ and $\delta\Omega_\nu = 0.05$ using our form for $P(k)$:

$$P_{\rm th}(k) = Ak^n\,[T(k)]^2\,. \tag{2.10}$$

We will vary the amplitude A by a factor of $2^{\pm 1}$ away from the COBE implied central value in 20 logarithmically spaced steps. However, since the definition of A is author dependent, we will discuss our results in terms of the parameter b_8 for each model. Thus we are effectively varying b_8 in a range centered on the COBE best fit b_8.

The value of b_I is somewhat more constrained than values of b_8. For the IRAS galaxies, separate determinations of b_I have been made by comparing their velocities and distributions. These dynamical tests yield the 95% confidence values $b_I = 1.16 \pm 0.42$ (Ref. [40]) and $b_I = 1.23 \pm 0.46$ (Ref. [41]). However, the POTENT analysis [22] of the Berkeley IRAS galaxies finds that the 95% confidence interval for $b_I = 0.5 - 1.3$. We therefore combine these measurements to say that $b_I = 1.1 \pm 0.3$ to cover the 95% confidence overlap region of the b_I determinations. We consider the measurement of $b_I = 1.1 \pm 0.3$ to be a *bona fide* data point, which we add to our χ^2 test. As is usual, we will assume a constant bias factor independent of scale and we will allow b_I to vary in seven linearly spaced steps between 0.8 and 1.4. We calculate S for each of the values of b_I and b_8, and find the set (b_I, b_8), which gives the lowest value of S, and plot the corresponding ΔS in our $\Omega_\nu - n$ contour plots. Some of these models, which have $b_I = 1.00$ are shown in Fig. 4.

We calculate the POTENT rms velocities by the same procedure as described in Ref. [10]. In our comparison of the rms POTENT velocities to theoretical rms velocities, we will incorporate the cosmic variance of the velocity field. The idea is that with a Gaussian density field, the velocity field will also be Gaussian. The magnitude of the velocity vector will have a χ^2 distribution with 3 degrees of freedom. The variance of the rms velocity is much larger than the POTENT velocity errors. For example the 68% theoretical confidence range on the average predicted velocity magnitude $\langle v \rangle$ corresponds to

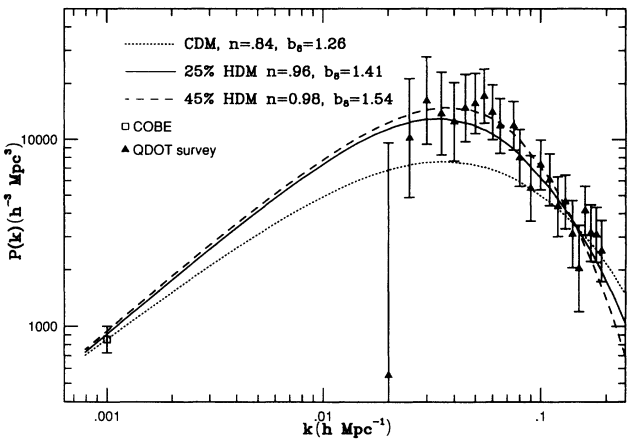

FIG. 4. Here we show the IRAS QDOT power spectrum data [27] and the COBE amplitude constraint [23] (converted to a redshift space power spectrum constraint for $b_I = 1.0$). The models shown have negligible gravity wave contributions to the COBE anisotropy, and have best fit normalizations $b_8 = 1.26$, 1.41, and 1.54 for the models shown with 0%, 25%, and 45% HDM, respectively. We have shown only half of the QDOT data so the plot is easier to read. The value of $n = 0.84$ yields the best-fitting CDM model without gravity waves. Note that simply tilting a CDM spectrum cannot reproduce the large scale "bump" in the IRAS power spectrum, which is generally why CDM models do not fare as well as C+HDM models.

$(\langle v\rangle - 0.48\langle v\rangle, \langle v\rangle + 0.32\langle v\rangle)$, while the POTENT errors are less than $\sim$ 15%. This is plotted in Fig. 3 for the $n = 0.96$, 25% HDM model. If we normalize an $n = 1.00$ power spectrum to COBE then the predicted velocities are within the POTENT 1σ error bars, regardless of the HDM fraction (see, e.g., $n = 1.00$, 50% HDM model in Fig. 3). As we decrease n below 1.00, we will decrease the predicted velocities well below the POTENT values. Thus the upper limit on the predicted velocity will be the most relevant quantity for comparing theory to observations. We combine this upper limit in quadrature with the POTENT 1σ error, and use this as a fairer estimate of the error bar in our S values.

While adding errors in quadrature is strictly correct only for Gaussian errors, the velocity distribution is not too far from a Gaussian. We plot several theoretical predictions for $\langle v\rangle$ against the POTENT velocities in Fig. 3. Even with these huge error bars, we find that the predicted velocities for models with significant gravity wave contributions will still have trouble matching the POTENT derived velocities.

D. Results of linear data analysis

The results of our test are presented in Figs. 5 and 6 for models without and with gravity waves, respectively. Starting with our absolute best-fitting model ($n = 0.98$, 25% HDM) and working outward, we plot five concentric curves with confidence levels of 25, 50, 68, 95, and 99 %. When one reaches the level of 50%, areas where the theory does not match the data become discernible in the data plots. The first thing to note about the graphs is that models with $n = 1.00$ do quite well for a large range

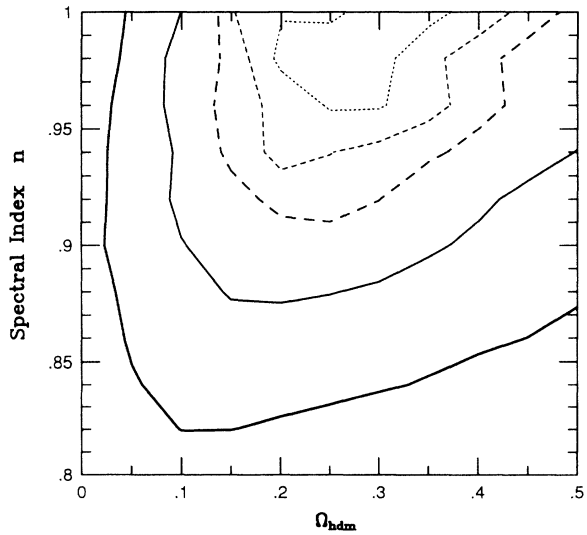

FIG. 5. $\chi^2(2)$ contours in the n-$\Omega_{\rm HDM}$ plane for models with a negligible gravity wave content. Moving outward from the center of the semicircular region on the graph are contours corresponding to 25% (dotted), 50% (dashed), 68% (heavy long dashed), 95% (solid), and 99% (heavy solid) confidence levels.

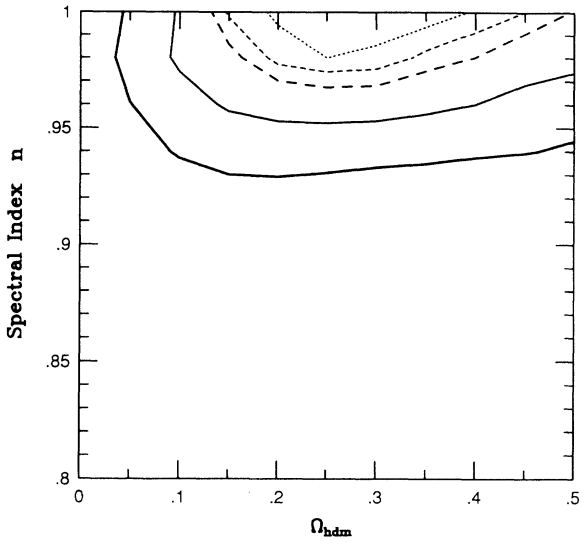

FIG. 6. $\chi^2(2)$ contours in the n-$\Omega_{\rm HDM}$ plane for models with gravity waves. Moving outward from the center of the top edge of the graph are contours corresponding to 25% (dotted), 50% (dashed), 68% (heavy long dashed), 95% (solid), and 99% (heavy solid) confidence levels.

of HDM fractions. This result supports earlier claims that $n = 1$ models normalized to COBE have sufficient power to explain "large-scale power" apparent in galactic clustering measures. If the measurement errors were smaller our test would be an even better discriminator of models.

We have two scenarios to discuss: models with and without gravity waves. First we point out one general trend, which is common to all models, and which does not show up in the ΔS plots. As we decrease n we decrease the amount of mass clustering power on small scales. To increase the galactic clustering power to compensate for this, one needs to increase the amount of galactic biasing b_I. Since our program finds the best-fit b_I, we will point out that small n models correspond to highly biased models (large b_I). We could better limit the models if we had more precise information about b_I.

The χ^2 contours for models with no gravity waves are shown in Fig. 5. The first feature noticeable in the plot is that models with $\Omega_{\rm HDM} \lesssim 0.05$ are ruled out at 99% confidence for any value of n. Next we note that all models with $n \lesssim 0.82$ are ruled out at the 99% confidence, independent of the HDM fraction. This limit rises from a minimum ($n \geq 0.82$) at $\Omega_{\rm HDM} = 0.1$ to the limit $n \geq 0.87$ for $\Omega_{\rm HDM} = 0.5$. This is easily understood since models with a lot of "tilt" already have little galaxy scale power, and large HDM fractions exaggerate this behavior. The region of best fit (confidence levels < 50 %) occurs in a roughly rectangular region $0.94 \lesssim n \lesssim 1.00$ and $0.15 \lesssim \Omega_{\rm HDM} \lesssim 0.45$ That these fits are quite good can be seen from the direct comparisons to data shown in Figs. 3 and 4 for a few models.

The χ^2 contours for models with gravity wave con-

tributions according to Eq. (2.5) are shown in Fig. 6. It is readily apparent that the allowed parameter space is much smaller. Again, models with $\Omega_{\rm HDM} \leq 0.05$ are again ruled out with 99% confidence. Here, though, the 99% confidence limit on n rules out models with $n \lesssim 0.93$. The region of best fit (<50% confidence levels) occurs in a roughly rectangular region $0.97 \lesssim n \lesssim 1.00$, $0.15 \lesssim \Omega_{\rm HDM} \lesssim 0.45$. Including significant amounts of gravity waves forces the normalization of the density power spectrum to be much lower, which depletes the amount of clustering power.

We note that our 99% confidence limit on n in models with gravity waves implies that $\gtrsim$80 % of the COBE signal is attributed to the effect of density fluctuations. This tells us that to fit large scale structure one requires that the COBE signal cannot be dominated by inflation generated gravity waves. Our best-fit models are those in which at least 90% of the COBE signal is due to density fluctuations. Our two conclusions from this analysis are that the power spectrum must be close to the Harrison-Zeldovich form ($n = 1.00$) and that the COBE signal must be mostly due to density fluctuations.

III. CONSTRAINTS FROM DATA ON NONLINEAR STRUCTURES

As noted in the preceding section, we find the best models still have a fairly large range of $\Omega_{\rm HDM}$. This is not surprising, since we have confined ourselves to only the largest scales, $k \lesssim 0.2h$ Mpc^{-1}, where the transfer functions for all the models do not differ much (see Fig. 1). The best place to discriminate between these models is on smaller scales, where we have data only on the nonlinear part of the power spectrum.

A. The data

The relation between nonlinear structures and the amplitude of the linear power spectrum is quite complicated, and it is nontrivial to extract strong conclusions from this data. We will consider two such constraints, which we feel can be used relatively safely—constraints on the amplitude of $\sigma(8h^{-1}$ Mpc) or equivalently b_8, and the requirement that quasars form early enough to be compatible with observations. The quasar constraint is a lower bound on the power spectrum amplitude while $\sigma(8h^{-1}$ Mpc) is an upper bound (at a somewhat larger scale).

1. High redshift quasars

The discovery of quasars with high redshifts (about 20 with $z \geq 4$) was a direct challenge to theories of structure formation. One needs a minimum amplitude for density fluctuation on galactic scales to account for the quasar population. Efstathiou and Rees (Ref. [42]) considered the formation of quasars in a highly biased ($b_8 = 2.5$) $n = 1$ CDM model. The basic strategy is that in order for a massive black hole to form and power the quasar emission, one first requires a host dark matter halo to supply the gravitational potential to induce baryonic infall. The number density of structures for a given power spectrum can be computed using Press-Schecter theory or the techniques in Ref. [51]. The number density of structures depends exponentially on a parameter ν given by

$$\nu = \frac{\sigma_c}{\sigma(R)} \tag{3.1}$$

where R is the radius of the initial collapsing region appropriate for the objects in question and σ_c is the linear theory value of $\sigma(R)$, which corresponds to the gravitational collapse and virialization of the object. Using the spherical collapse approximation (see Appendix A) $\sigma_c = 3(12\pi)^{2/3}/20 = 1.69$. In this application we use the Gaussian filtered mass fluctuation $\sigma_G(R)$

$$\sigma_G(R)^2 = \frac{1}{2\pi^2}\int dk k^2 P(k) e^{-k^2R^2} , \tag{3.2}$$

where the subscript "G" is to remind us that we are using a Gaussian filtering function. The parameter ν then has the physical meaning of the ratio of the overdensity in a collapsed object to the ambient rms overdensities. Thus specifying ν tells us the amplitude of the density fluctuations on the scale R. Also, since the calculated number density depends exponentially on ν, it is hoped that errors in the measured number density will not significantly change the value of ν.

Efstathiou and Rees (Ref. [42]) estimated that the minimum mass for a quasar halo was $\geq 2\times10^{12}M_\odot$ ($h = 0.5$). They found that a $b_8 = 2.5$, $n = 1$ CDM model could account for the number density of quasars at least out to a redshift of $z = 5$. Haehnelt and Rees (Ref. [43]) improved on this treatment by showing that the $b = 2.5$ CDM could fit the quasar luminosity function at a variety of redshifts. Since both increasing the HDM fraction and reducing n lessen the amount of power on small scales, it is obvious to ask whether the amplitude of quasar scale fluctuations has decreased below that required for making quasars. Haehnelt (Ref. [11]) used the techniques of Ref. [43] to limit the HDM fraction in $n = 1$ models and n in CDM models, finding that $n > 0.75$ in CDM models and the HDM fraction must be $\Omega_{\rm HDM} \leq 0.3$. Schaefer and Shafi (Ref. [10]) showed that 25% HDM and $n = 0.94 - 0.97$ is compatible with the quasar density out to a redshift of $z \sim 5$.

The Press-Schecter technique is, however, not without errors. Even if we knew the quasar number density perfectly, and hence could deduce the exact value of ν, there would still be uncertainties. These uncertainties have been discussed before in a variety of places. Here we follow the discussion of Ref. [24]. The uncertainties in ν can be found by

$$\Delta \ln\nu = \Delta \ln\sigma_c - \frac{d\sigma(R)}{dR}\frac{dR}{dM}\Delta \ln M. \tag{3.3}$$

First of all it is not clear what value of σ_c to use. While most authors use the value 1.69, comparison of Press-Schecter results to N-body simulations imply values of

σ_c anywhere from 1.33 [42] to 1.69 [44]. To bracket these values we can assume $\sigma_c = 1.5 \pm 0.2$. Second there are errors in the quoted mass of the object. The theoretical value for the quasar halo mass is somewhat uncertain, and the mass of the object derived from the luminosity function comes with an additional error. To evaluate the total uncertainty one needs to know the value of $[d\sigma(R)/dR](dR/dM)$. For the quasar halo mass of $2 \times 10^{12} M_\odot$, the Gaussian filter radius is $R = 0.6h^{-1}$ Mpc. For $n = 1$ models $[d\sigma(R)/dR](dR/dM)$ ranges from 0.14 for CDM models to 0.033 for 50% HDM. Assuming a factor of 3 error in the observational and theoretical masses, we then have

$$\Delta \ln \nu = \pm 0.13 \pm 0.04 \pm 0.04 \tag{3.4}$$

for 50% HDM ($n = 1$), which has the smallest uncertainties of the $n = 1$ models. We conclude that there could be an uncertainty of about 20% in the amplitude of the density fluctuation $\sigma(R)$ derived from the quasar density.

In order to have the proper quasar density at early redshifts, one needs to have $\sigma(0.6h^{-1}\ \text{Mpc}) \geq 1.1$ today (using $\sigma_c = 1.5$). The effect of the hot dark matter on the growth of density fluctuations at these scales changes the above threshold value by only a few percent [11]. To forbid models, which are unlikely to have quasars form early enough, we make the replacement

$$S \to S + 20 \left[\frac{\sigma(0.6h^{-1}\text{Mpc}) - 1.1}{0.22} \right]^2 \tag{3.5}$$

whenever $\sigma(0.6h^{-1}\text{Mpc}) \leq 1.1$. We have weighted this contribution to S by 20 to strongly penalize models without sufficient small scale power. Since there are about 40 data points in our χ^2 analysis an amplitude $\sigma(0.6h^{-1}$ Mpc), which is 40% (like two standard deviations) smaller than our threshold amplitude will cause ΔS to be so large that the model will be ruled out by the quasar data alone. Decreasing the penalty factor will loosen our constraints on high HDM fraction and low n models. Increasing the penalty will drive us closer to the limits usually quoted ($\Omega_{\text{HDM}} \leq 0.30$, or $n > 0.75$ for $\Omega_{\text{HDM}} = 0$ [10,11]).

2. $\sigma(8h^{-1}$ Mpc)

Since it has become traditional to specify the amplitude of linear theory by b_8, some attention has been paid to determining the value of b_8 from observations. There are several ways of getting at this quantity, which seem to be converging on the range $b_8 = 1.5 - 2.0$ for the $\Omega = 1$ models. We will consider some of the more recent attempts to constrain this parameter.

The easiest way to estimate the density fluctuations is by finding the variance of the galactic number density. For the IRAS galaxies we have two estimates of the number density fluctuations: one from the QDOT survey [45]

$$b_I \sigma^{\text{nonlinear}}(8h^{-1}\ \text{Mpc}) = 0.69 \pm 0.09\ , \tag{3.6}$$

which is in perfect agreement with the estimate from the Berkeley survey [46]

$$b_I \sigma^{\text{nonlinear}}(8h^{-1}\ \text{Mpc}) = 0.69 \pm 0.04\ . \tag{3.7}$$

The error on the averaged combined measurement is essentially the same as the Berkeley error, $b_I \sigma^{\text{nonlinear}}(8h^{-1}\ \text{Mpc}) = 0.69 \pm 0.04$. The 95% confidence upper limit is then $b_I \sigma^{\text{nonlinear}}(8h^{-1}\ \text{Mpc}) \leq 0.77$ If we take an extremely small value for $b_I = 0.5$, which is the POTENT 95% confidence lower limit, this would imply that $\sigma^{\text{nonlinear}}(8h^{-1}\ \text{Mpc}) \leq 1.54$. If we use the spherical collapse model (see Appendix B) to determine what that means in terms of the linear density fluctuation, this implies

$$\sigma^{\text{linear}}(8h^{-1}\ \text{Mpc}) \leq 0.71 \text{ or } b_8 \geq 1.40. \tag{3.8}$$

To be extra cautious, we will adopt the constraint

$$\sigma^{\text{linear}}(8h^{-1}\ \text{Mpc}) \leq 0.80 \text{ or } b_8 \geq 1.25 \tag{3.9}$$

for a new round of χ^2 testing.

A few remarks are in order here concerning the value of b_8. Early investigations found that CDM models with $n = 1$ required values of $b_8 \sim 2 - 3$ [47] to get agreement with galactic velocity dispersion data and correlation functions. However, large scale structure data required that CDM have smaller values of b_8. It was postulated that dynamic effects, especially "velocity bias" [48] might accommodate smaller values of b_8. High-resolution simulations [49], however, find $b_8 \geq 1.4$, despite their confirmation of the existence of the velocity bias effect. This conclusion seems to also hold for $n < 1.00$ [50]. Reference [50] also suggests that this is true even in models with C+HDM. However, they did not consider the effect of the dynamical effects of HDM in their study, and this seems to allow us to use $b_8 < 2$ with significant amounts of HDM [12–14]. No systematic study has been done to determine what values of b_8 are allowed, although $b_8 = 1.5$ seems to work with $n = 1.00$, $\Omega_{\text{HDM}} = 0.30$. Our constraint $b_8 \geq 1.25$ seems to be easily consistent with these case studies.

Another constraint on the mass fluctuation amplitude comes from cluster properties. Since clusters are a few Mpc in size, they are an almost ideal choice for determining b_8. However, to determine the number density of cluster mass structures analytically, one must use a procedure such as the "BBKS" method [51] or the Press-Schecter [52] model. There are some uncertainties associated with this technique however, which we have discussed in the preceding section on quasars. In Ref. [6] it was found that $b_8 = 1.12 - 0.96$ for models with 0–50% HDM, based on $R \geq 0$ Abell cluster number abundance. To arrive at this number van Dalen and Schaefer (Ref. [6]) used the spherical collapse model. The $R = 0$ Abell clusters are the poorest Abell clusters and represent initially weaker density fluctuations. The smaller amplitude density fluctuations tend to be highly asymmetric [51] and collapse faster than spherical perturbations (see, e.g., Ref. [53]), so a spherical collapse model probably gives b_8 values that are too small. It was estimated that more ac-

curate values for b_8 would be at least 30% larger, i.e., $b_8 = 1.46 - 1.25$, consistent with the adopted restriction $b_8 \gtrsim 1.25$.

Perhaps a more reliable way to study the mass fluctuations in clusters is to select them by their x-ray temperatures, as this gives a direct indication of the gravitational mass potential. These studies tend to give results consistent with much higher b_8, implying $b_8 \sim 2.0 - 2.5$ [54], $b_8 = 1.6 - 1.9$ [44], and $b_8 = 2.0$ [55]. Thus we find our restriction $b_8 \geq 1.25$ is, if anything, too conservative.

B. Results of nonlinear analysis

In Figs. 7 and 8 we again plot the χ^2 contours for models with and without significant gravity wave temperature anisotropies. We note that because our method of enforcing the nonlinear constraints is somewhat *ad hoc*, the contours in Figs. 7 and 8 no longer have a clear statistical meaning. We believe that the "allowed region" in our graph is perhaps larger than the data really allow because we have been quite conservative in our treatment of these limits. The effect of the nonlinear constraints is quite clear. The restriction $b_8 \geq 1.25$ forces the normalization of small $\Omega_{\rm HDM}$, $n \sim 1$ models to be too low to match the large scale structure data. This is symptomatic of the CDM models, which, when normalized to COBE, have too much small scale power. The effect of enforcing the lower limit on the amplitude from quasars is to cut out a triangle of parameter space corresponding to large $\Omega_{\rm HDM}$ and small n. This is symptomatic of $\Omega_{\rm HDM} \sim 1$ model problems, there being not enough small scale power to explain the early epoch of quasar formation. If we had increased the penalty for violating the quasar formation limit, we would shift the limit contours on high $\Omega_{\rm HDM}$ to the left of the graph, but not past $\Omega_{\rm HDM} \leq 0.30$ for $n = 1.00$.

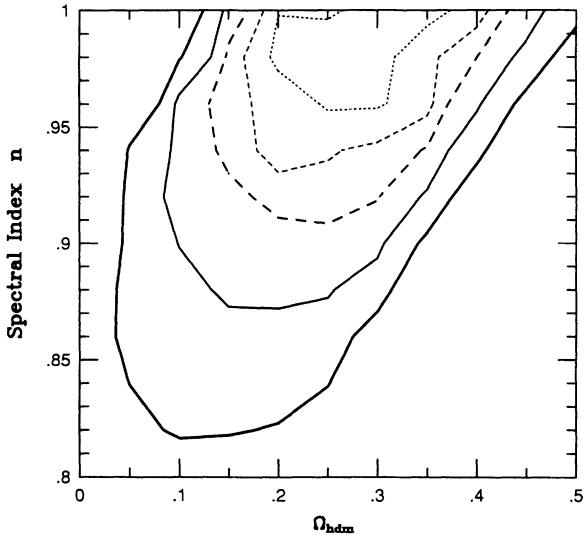

FIG. 7. Same as Fig. 5, but we have added the constraints from nonlinear data. We have added the restriction that $b_8 \geq 1.25$ and that we have sufficient power for quasar formation. The procedure for adding these constraints in a χ^2 analysis is described in the text. The significance of the contours is here not well defined because of the way we have added the nonlinear constraints.

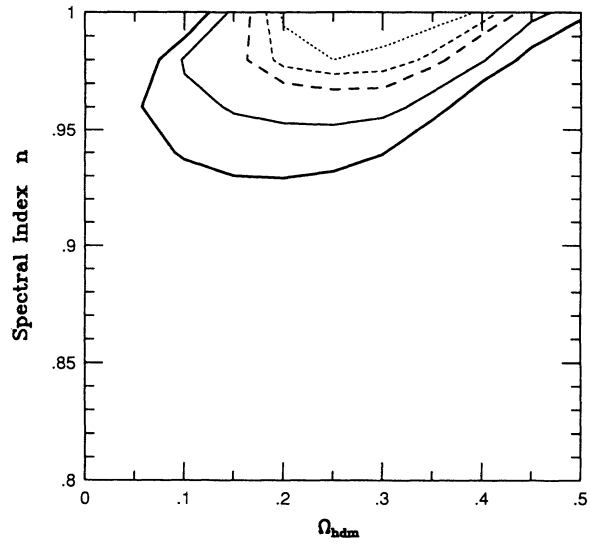

FIG. 8. Same as Fig. 6, but we have added the constraints from nonlinear data. We have added the restriction that $b_8 \geq 1.25$ and that we have sufficient power for quasar formation. The significance of the contours is here not precise because of the way we have added the nonlinear constraints.

What we are left with is a patch of parameter space which has $n \sim 1$ and $\Omega_{\rm HDM} = 0.25 \pm 0.15$. This is in agreement with earlier studies and shows that models with $\Omega_{\rm HDM}/\Omega_{\rm CDM} \sim 1/3$ are significantly better fits to the data than with no HDM. The range of n is roughly the same as in the linear analysis, although the nonlinear quasar constraint has effectively chopped off the low-n, high-HDM fraction corner of parameter space of the previous best fits. Our allowed region of parameter space overlaps the allowed region found by Liddle and Lyth (Ref. [56]). However, their analysis took the nonlinear constraints of Refs. [11,44] at face value so their allowed region is somewhat smaller than ours. They noted however, that their allowed region was meant to be suggestive of trends in the data and should not be taken literally. On the other hand we are taking pains to be overconservative with nonlinear constraints in the hope that our limits will be firmer.

Thus we find the following properties, which it is desirable for inflation to have. We require a density perturbation spectrum, which is quite close to a Harrison-Zeldovich spectrum as the data do not seem to favor much "tilting." For models with a negligible gravity wave contribution to the COBE signal, the best fits occur for $0.93 \lesssim n \lesssim 1.00$. In models with some gravity wave contribution, we find an even tighter range of best-fit n values, namely, $0.97 \lesssim n \lesssim 1.00$. Since we used Eq. 2.5 to determine this, we see that for $n = 0.97$ the gravity wave contribution to COBE is only 10%. Thus the data favor models for which density perturbations are $\gtrsim 90\%$ responsible for the COBE signal. We also find

$0.15 \lesssim \Omega_{\rm HDM} \lesssim 0.45$ gives the closest fits to the data, which implies we would nominally like one flavor of neutrino with a mass $m_\nu = 3 - 10$ eV. (The best fits imply a narrower range $\Omega_{\rm HDM} = 0.20 - 0.35$ implying $m_\nu = 4 - 8$ eV with $h = 0.5$.) With these attributes in mind we proceed to explore possible models for inflation.

IV. MODELS OF INFLATION

Grand unified theories (GUT's) provide the simplest framework for implementing the inflationary scenario. Although supersymmetric GUT's are currently more popular, for completeness we will also consider the ordinary nonsupersymmetric versions. The simplest example of the latter is provided by SO(10) with an intermediate mass scale. The minimal nonsupersymmetric SU(5) model is excluded both by the precise determination of $\sin^2\theta_W$ and by proton decay experiments. This is just as well from our point of view, since, as observed a decade ago [57], non-SUSY SO(10) models with an intermediate (B-L breaking) scale $M_{B-L} (\sim 10^{12}$ GeV) strongly suggest that the τ neutrino mass is in the eV range. The presence of a U(1) axion symmetry not only resolves the strong CP problem but also provides the cold dark matter component.

Two versions of the inflationary scenario, "new" and "chaotic," are readily realized in GUT's. The spectral index n of density fluctuations in the simplest realistic models typically lies between 0.96 and 0.92, although in some versions of chaotic inflation with SUSY GUT's, n could be as low as 0.88. Values of n much smaller than this are not particularly well motivated, both from the point of view of model building as well as observations of the large scale structure.

A. Inflation with nonsupersymmetric SO(10)

For definiteness, let us consider the following breaking:

$$\mathrm{SO}(10) \underset{M_X}{\longrightarrow} \mathrm{SU}(4)_c \times \mathrm{SU}(2)_L \times SU(2)_R \underset{M_{B-L}}{\longrightarrow} \mathrm{SU}(3)_c \times \mathrm{SU}(2)_L \times U(1)_Y M_X M_{B-L} \ .$$

A recent two-loop renormalization-group calculation involving the gauge couplings gives [58] $M_X \sim 10^{15} - 10^{16}$ GeV and $M_{B-L} \sim 10^{12\pm1}$ GeV, consistent with the measured values of $\alpha_c(M_Z)$ and $\sin^2\theta_W(M_Z)$.

A simple version of the seesaw mechanism for neutrino masses [59] suggests the hierarchy:

$$m_{\nu_1} : m_{\nu_2} : m_{\nu_3} \approx m_u^2 : m_c^2 : 10^{-1} m_t^2 . \tag{4.1}$$

One can of course design other models for which the above relation does not hold, but we will confine our attention here to just this simplest version. Here the three mass eigenstates ν_1, ν_2, and ν_3 primarily consist of ν_e, ν_μ, and ν_τ, respectively, and we have assumed (see below) that the heavy (right-handed Majorana) neutrino associated with the third family is a factor 10 (or so) heavier than the other two.

The Mikheyev-Smirnov-Wolfenstein (MSW) interpretation of the solar neutrino data suggests [60] that the ν_2 mass is $\sim 10^{-2.7} - 10^{-2.5}$ eV. With $m_t(m_t) \sim 130 - 150$ GeV, as suggested by recent analyses of the electroweak data, we expect the ν_3 (essentially ν_τ, with some admixture of ν_μ and ν_e) mass to be $\sim 5 - 10$ eV. [Without the numerical factor in Eq. (4.1), this mass would exceed the cosmological bound.] Note that according to this simple SO(10) example, unless the $\nu_\tau - \nu_\mu$ mixing happens to be tiny, the two-neutrino oscillation experiments by the CHORUS and NOMAD Collaborations should determine whether or not the "τ" neutrino is cosmologically significant.

The SO(10) model with the above symmetry-breaking chain suggests the existence of some dark matter in the form of τ neutrino. However, two essential ingredients are still missing, implementation of inflation and a candidate for cold dark matter (CDM). [Recall that inflation with only hot dark matter (HDM) does not seem compatible with the observed large scale structure, especially galaxy formation.] The simplest way to incorporate CDM here is to invoke a U(1) axion symmetry [61] broken at a scale around $10^{11} - 10^{12}$ GeV. Both the axions and neutrinos are then cosmologically significant. It may be useful to reiterate how this has come about. In nonsupersymmetric SO(10), an intermediate scale is needed to bring about consistency with the measured value of $\sin^2\theta(M_Z)$ as well as with the lower limits on the proton lifetime. This forces the gauged $B - L$ symmetry to break at an intermediate scale, which, for the above chain, is about $10^{12\pm1}$ GeV. Coupled with the seesaw, this strongly suggests that the τ neutrino mass ($\sim m_t^2/M_{B-L}$) is in the eV range. That is, the neutrino is a significant component of the dark matter. Cold dark matter is then needed to reconcile the inflationary scenario with observations related to large scale structure.

As far as inflation is concerned, the most straightforward scenario is realized by introducing a weakly coupled gauge singlet field ϕ in the manner of Shafi and Vilenkin [62]. The part of the potential, which drives (new) inflation is given by

$$V(\phi) = \lambda\phi^4 \left[\ln\left(\frac{\phi^2}{M^2}\right) - \frac{1}{2} \right] , \tag{4.2}$$

where M denotes the vacuum expectation value (vev) of ϕ. The quantity λ can be reliably estimated by considering the contribution of the scalar perturbations to the microwave background quadrupole anisotropy and identifying it with COBE's determination of $Q_{\rm rms\text{-}PS}$. [Note that for the potential in (4.2), the spectral index $n \approx 0.94$, and the tensor contribution to the anisotropy is negligible.]

One has (the subscript S denotes the scalar contribution)

$$\left(\frac{\Delta T}{T}\right)_S^2 \simeq \frac{32\pi}{45} \frac{V^3}{V'^2 M_P^6}\bigg|_{k\sim H} \tag{4.3}$$

where $M_P (= 1.2 \times 10^{19}$ GeV) denotes the Planck scale, and the right-hand side is to be evaluated when the scale

k^{-1}, corresponding to the present horizon size, crossed outside the horizon during inflation. Equation (4.3) can be rewritten as

$$|\Delta T/T|_S \simeq 0.067\sqrt{\lambda}N_H^{3/2}|\ln(\phi_H^2/M^2)|^{\frac{1}{2}} , \qquad (4.4)$$

where N_H (≈ 55) denotes the number of e foldings experienced by this scale, and ϕ_H is the field value when the scale crossed outside the horizon.

The logarithmic factor in (4.4) is of order 1–10, assuming that the vacuum energy density that drives inflation is comparable to M_X^4. For $M_X \sim 10^{15.5}$ GeV, $M \sim M_P = 1.2\times 10^{19}$ GeV, and taking $(\Delta T/T)_{\rm COBE} \approx 6\times 10^{-6}$, the fundamental quantity λ is estimated to be

$$\lambda \approx 2.2\times 10^{-14} . \qquad (4.5)$$

Any inflationary scenario is incomplete without an explanation of the origin of the observed baryon asymmetry in the universe. In the present case the inflaton mass $m_\phi \approx 10^{12.5}$ GeV, and so the basic idea is to create an initial lepton asymmetry via inflaton decay into one or more species of the heavy ("right-handed") majorana neutrinos. The appearance of "sphaleron" induced processes at the electroweak scale converts a specified fraction of this asymmetry into the observed baryon asymmetry. Details of how a satisfactory scenario is realized along these lines can be found in Ref. [63]. We mention here a few salient features.

(i) The reheat temperature $T_r \sim 10^{8.5}$ GeV so that the out of equilibrium condition on the "heavy" ($\sim 10^{12}$ GeV) neutrinos is readily satisfied.

(ii) The requirement that for temperature below T_r the rates for lepton number violating processes ($\nu\nu \leftrightarrow H^{0*}H^{0*}$ and $\nu H^0 \leftrightarrow \bar{\nu}H^{0*}$, where H° is the electroweak scalar Higgs boson) be smaller than the expansion rate ($H \simeq 20T^2/M_P$, where H denotes the Hubble constant) of the Universe, leads to the following constraint on the light neutrino masses [64]:

$$m_\nu \lesssim \frac{4 \text{ eV}}{(T_r/10^{10} \text{ GeV})^{\frac{1}{2}}} \approx 20 \text{ eV} . \qquad (4.6)$$

This is fully consistent with a cold plus hot dark matter scenario where neutrinos in the mass range $3-10$ eV are needed.

(iii) In the present approach the colored scalar triplets, which mediate proton decay are not needed for baryogenesis and consequently are allowed to have masses $\sim M_X$.

(iv) Finally, it is possible, following Ref. [65], to identify the inflaton with the field that spontaneously breaks the axion symmetry. This would make for a more economical approach.

(v) With an appropriate reinterpretation, the chaotic inflationary scenario can be realized within the framework of this SO(10) model. The ratio of the scalar to the tensor contribution in this case is

$$(\Delta T/T)_T^2/(\Delta T/T)_S^2 \simeq 0.22. \qquad (4.7)$$

B. Supersymmetric inflation

The presently measured gauge couplings of the standard model, when extrapolated to higher energies with supersymmetry (SUSY) broken at scales around 10^3 GeV [66], appear to merge at scales around 10^{16} GeV. This is a boost for supersymmetric GUT's, with SU(5) or SO(10) being the obvious gauge groups. In the presence of unbroken matter parity, either of them can provide a cold dark matter candidate in the form of a lightest supersymmetric particle (LSP). However, hot dark matter in the form of massive neutrinos most naturally appear in the SO(10) model. The supersymmetric SO(10) scheme has some additional features, which make it attractive from the particle physics viewpoint.

(a) A Z_2 subgroup of the center of SO(10) [more precisely spin (10)] is left unbroken if tensor representations are employed to do the symmetry breaking. This Z_2 symmetry [67], which is not contained in $SU(3)_c\times SU(2)_L\times U(1)_Y$, acts precisely as matter parity.

(b) In some versions of SUSY SO(10), the important parameter $\tan\beta$ ($\equiv \phi^u/\phi^d$, the ratio of the two VEV's which provide masses to "up" type and "down" type quarks) is predicted to lie close to m_t/m_b [68]. One consequence of this is the identification of the "bino" [the supersymmetric partner of the $U(1)_Y$ gauge boson] as the LSP, with mass $\sim 200-300$ GeV.

(c) Fermion mass ansatzes have recently attracted a fair amount of attention and are most simply realized within the framework of SO(10) [69].

To summarize, particle physics considerations as well as observations of large scale structure, which favor a cold plus hot dark matter scenario, together suggest SUSY SO(10) as an attractive way to proceed. Inflation, either new or chaotic, can be implemented by introducing a suitable singlet superfield. Remarkably enough, singlets are typically employed to achieve the breaking of the GUT's symmetry (without breaking SUSY), and we exploit one of them to induce inflation.

Let Φ denote the SO(10) singlet (inflaton) superfield, $\chi(\bar{\chi})$ are the Higgs superfields in the 126 ($\overline{126}$) representations whose VEV's provide Majorana masses to the right-handed neutrino, and $16_i (i=1,2,3)$ are the matter superfields. To simplify the discussion, we restrict attention to the sector involving an interplay only between these superfields. This allows us to discuss the salient features of the (chaotic) inflationary scenario including baryogenesis. Consider the renormalizable superpotential

$$W = \alpha\Phi(\chi\bar{\chi} - M_X^2) + \frac{M}{2}\Phi^2 + \frac{\beta}{3}\Phi^3 + \gamma_{ij}16_i16_j\bar{\chi} . \qquad (4.8)$$

Note that $\Phi \to \Phi$ under the matter parity contained in SO(10) (similarly $\chi, \bar{\chi} \to \chi, \bar{\chi}$, and $16_i \to -16_i$).

The superpotential W gives rise to a supersymmetric ground state in which (VEV's refer to the scalar components of the superfields)

$$\langle\phi\rangle = 0,\ \langle 16_i\rangle = 0, \qquad \langle\chi\rangle = \langle\bar{\chi}\rangle^* \neq 0. \tag{4.9}$$

It is clear that matter parity is unbroken, and we expect the LSP to contribute to the cold dark matter component.

Even though B-L is now broken at $M_X \sim 10^{16}$ GeV, the right-handed τ neutrino mass must be of order $10^{12} - 10^{13}$ GeV, if the "light" τ is to be the dark matter component. The inflaton must be at least twice as heavy, and one simple way to have $m_\phi \sim 10^{13}$ GeV is to arrange the coefficients α and M in (4.8) to be of order m_ϕ/M_X and m_ϕ, respectively. The decay rate of the inflaton into right-handed neutrinos is given by

$$\Gamma \sim \frac{1}{4\pi}\left(\frac{m_\phi}{M_X}\right)^6 m_\phi \text{ GeV} . \tag{4.10}$$

With $m_\phi \sim 10^{13}$ GeV, the reheat temperature T_r is of order 10^6 GeV. Baryogenesis via leptogenesis now proceeds along the lines given in Ref. [63]. Note that because of the relatively low T_r, the otherwise vexing gravitino problem is neatly avoided in this approach.

Depending on the details, the spectral index n lies between 0.94 (if the quartic potential dominates) and 0.96 (with a quadratic potential dominant during the chaotic inflationary phase). The ratio $(\Delta T/T)_T^2/(\Delta T/T)_S^2 \simeq 0.22$ and 0.11, respectively.

C. Inflation without the singlet

The question we wish to address here is the following: Is it possible to implement inflation with GUT's without the gauge singlet? Surprisingly perhaps [70], an affirmative answer appears possible for a special class of supersymmetric GUT's in which, up to a normalization constant, the GUT scale is determined in terms of M_S and M_P, the SUSY breaking scale and the Planck scale respectively. Moreover, the normalization constant is fixed from the quadrupole anisotropy. Such models [71] naturally arise after compactification of the ten-dimensional $E_8 \times E_8$ heterotic string theory [72], and models based on $G \equiv \mathrm{SU}(3)_c \times \mathrm{SU}(3)_L \times \mathrm{SU}(3)_R$ or its subgroups provide some elegant examples. The scalar fields needed to spontaneously break G to $\mathrm{SU}(3)_c \times \mathrm{SU}(2)_L \times \mathrm{U}(1)$ can be used to drive inflation.

The key ideas are relatively straightforward and perhaps best illustrated by a simplified example. Consider a rank five gauge symmetry $H \equiv \mathrm{SU}(3)_c \times \mathrm{SU}(2)_L \times \mathrm{U}(1)_Y \times \mathrm{U}(1)'$, where the extra factor $\mathrm{U}(1)'$ is to break at some superheavy scale M (below M_P). Let $\phi, \bar{\phi}$ denote the pair of Higgs scalars whose vev's do this breaking. Note that $\langle\phi\rangle = \langle\bar{\phi}\rangle^*$ so that the D term vanishes. Since the only independent dimensional parameters are M_S and M_P (M is determined in terms of them), the $\Phi\bar{\Phi}$ terms in the superpotential are either absent or carry coefficients of order M_S. (Here $\Phi, \bar{\Phi}$ denote the corresponding superfields.) Moreover, in order to ensure F flatness, the cubic couplings $\Phi^3, \bar{\Phi}^3$ are also absent [otherwise $\mathrm{U}(1)'$ would break at scales $\sim M_S$].

In the absence of SUSY breaking the superpotential W is taken to be

$$W = h\chi\chi\Phi + \frac{\kappa}{M_P}(\Phi\bar{\Phi})^2 + \cdots \tag{4.11}$$

where χ denotes some matter superfield with the coupling h of order unity. Assuming a radiative breaking scenario along the lines envisaged in supergravity models with electroweak breaking, the effective potential takes the generic form

$$V(\phi, \bar{\phi}) \sim -M_S^2|\phi|^2 + \kappa^2\frac{|\phi|^6}{M_P^2} . \tag{4.12}$$

Minimization of (4.12) leads to the result

$$M \equiv |\langle\phi\rangle| = |\langle\bar{\phi}\rangle| \sim \kappa^{-\frac{1}{2}}(M_S M_P)^{\frac{1}{2}} . \tag{4.13}$$

Provided that κ^2 is sufficiently small, the potential in (4.12) will yield a satisfactory (chaotic) inflationary scenario. It turns out that $\kappa \sim 10^{-7}$ (from COBE), which gives $M \simeq 10^{15}$ GeV. The spectral index $n \approx 0.92$, while the ratio of the tensor to the scalar quadrupole anisotropy is $(\Delta T/T)_T^2/(\Delta T/T)_S^2 \approx 0.4$. Values of $n \approx 0.88$ (but no lower) can be entertained within this framework. This is just as well, since our analysis in the earlier sections seems to favor the range $1.0 \gtrsim n \gtrsim 0.9$.

To summarize, grand unification provides an elegant framework for implementing both the new and chaotic inflationary scenarios. Some popular models based on SO(10) or $\mathrm{SU}(3)_c \times \mathrm{SU}(3)_L \times \mathrm{SU}(3)_R$ predict the value of the spectral index n in the range 0.96 to 0.92. Cold dark matter, in axions and/or LSP, as well as hot dark matter in massive neutrinos are readily incorporated in these schemes.

V. CONCLUSIONS

We have performed a χ^2 test of the hot dark matter fraction Ω_{HDM} and spectral index n in the predicted linear theory power spectra with data on scales ranging from 1 to 10^4 Mpc, mainly from the COBE satellite and the QDOT IRAS survey of galaxies. We find that the inflation based scenario of large scale structure formation, in which the dark matter consists of cold plus hot components, can provide a good fit to large scale structure data.

Taking the primordial power spectrum to have spectral exponent n, we find with 99% confidence, respectively, that $n \gtrsim 0.82$ ($n \gtrsim 0.94$), in models with (without) significant gravity wave contributions to the COBE anisotropy. The precise bound depends slightly on the HDM fraction. We find in models with a significant gravity wave anisotropy, that the COBE signal must contain a contribution of less than 20% from the gravity waves.

Although pure CDM models are a considerably worse fit to the data than C+HDM models, if one insists on only one type of dark matter, i.e., CDM, the best fits are

for $n = 0.84$ ($n = 0.92$) in models without (with) gravity waves, respectively.

The best fit region for all data, including some constraints from non-linear structure, is roughly a tilted rectangle (see Figs. 7 and 8). For models with negligible gravity wave anisotropies, we obtain limits on $\Omega_{\rm HDM}$, which depend on n, roughly $\Omega_{\rm HDM} \approx 0.30 - 1.2(1-n) \pm 0.15$, for $n \geq 0.87$ (95% confidence limits). For models with a large tensor COBE anisotropy, the tilted rectangle extends for a shorter range of n, implying $\Omega_{\rm HDM} \approx 0.30 - 2.5(1-n) \pm 0.15$, for $n \geq 0.95$ (95% confidence limits). Thus, the best fits occur for $\Omega_{\rm HDM} \sim 0.15 - 0.35$, with n very close to unity.

Realistic examples of inflation from grand unification theories, including both supersymmetric and ordinary GUT's, which have these properties have been presented. These models are also consistent with other cosmological and particle physics constraints.

Note added in proof. Since we submitted this paper we have extended our analysis to include values of $n > 1$. We find that $n < 1.17$ with 99% confidence regardless of the dark matter composition and that $\Omega_{\rm HDM}$ must always be less than 0.6 even with $n > 1$. If we allow the Hubble parameter h to vary from 0.5 we find that the best fit values of n and $\Omega_{\rm HDM}$ change; smaller n and larger HDM fractions are favored when $h > 0.5$ and larger n and smaller HDM fractions are favored for $h < 0.5$. Pure CDM models are allowed when h is as small as 0.3, but for $h \geq 0.4$ we find $\Omega_{\rm HDM} > 0$ at 95% confidence. Thus for the canonical range of Hubble values $0.4 < h < 0.6$ a mixture of cold and hot dark matter is required to fit the observations.

ACKNOWLEDGMENTS

We wish to thank Hume Feldman for supplying us with the IRAS $P(k)$ and Michael Strauss for interesting discussions. We also thank Ned Wright for informing us of the Yoram Avni article and for many useful comments on our manuscript. This work was supported by NASA (Grant No. NAGW - 1644) and DOE (Grant No. DE-FG02-91ER40626).

APPENDIX A: TRANSFER FUNCTION CALCULATIONS

As described in Ref. [3], we integrate the Fourier space evolution equations in (conformal) time using the gauge-invariant variables for the density Δ_{ca} and velocity V_a perturbations in each energy density component (CDM, neutrinos, photons, and baryons) as given in Ref. [73]. Here we integrate the equations in conformal time instead of the scale factor as we had done previously. We begin the integration well before the matter dominated era ($z = 8.3\times10^6$) and integrate up until the present time ($z = 0$). We have used only one flavor of massive neutrino, with the other two flavors essentially massless. For the baryon equations we use the equations for the difference between the baryon and photon density and velocity perturbations [the variables $S_{\rm br} \equiv \Delta_{c,\rm baryon} - (3/4)\Delta_{\rm cr}$ and $V_{\rm br} \equiv V_{\rm baryon} - V_r$ given in Ref. [73], Sec. II-5]. For the massive neutrinos we use the imperfect fluid treatment of Ref. [74]. We numerically integrate the equations using a Haming predictor-corrector routine as we have found it tracks the oscillations of the relativistic components more accurately than Bulirsch-Stoer or Runge-Kutta routines. After recombination is completed ($z = 900$) we switch from integrating the baryon-photon difference equations to simply integrating the baryon and photon component ($\Delta_{c,\rm baryon}$, $\Delta_{\rm cr}$ and $V_{\rm baryon}$, V_r) equations separately.

TABLE I. Transfer functions with $\Omega_{\rm baryon} = 0.05$, $h = 0.5$.

Ω_ν	t_1	t_2	t_3	t_4	t_5
0.00	-1.150	29.60	48.49	-43.17	132.4
0.05	-0.8654	17.65	165.1	-277.1	343.4
0.10	-0.2942	1.393	274.6	-472.6	538.2
0.15	0.1157	-8.820	330.0	-541.4	660.8
0.20	0.3176	-12.69	334.9	-495.8	726.1
0.25	0.3128	-10.60	296.3	-361.6	756.5
0.30	0.1363	-3.540	219.1	-142.9	771.2
0.35	-0.1454	6.144	127.6	78.64	840.3
0.40	-0.4276	15.15	53.35	193.1	1084
0.45	-0.6522	21.44	15.98	131.2	1582
0.50	-0.7882	24.04	25.49	-147.3	2395

We have checked the results of our code by comparing our baryonic transfer functions against those of Ref. [4] who gives values for $\Omega_{\rm baryon} = 0.1$ and 0.01 and found good agreement, although here we present results only for $\Omega_{\rm baryon} = 0.05$. We have fit the transfer functions to an inverse fifth order polynomial and the results are given in Table I. We find a fifth-order inverse polynomial works a little better for C+HDM models than a fourth-order one, as is more usual for CDM models. The transfer functions given here are not baryonic transfer functions, but rather are fits to the total density perturbation (i.e., $\Delta = \Omega_{\rm CDM}\Delta_{c,\rm CDM} + \Omega_\nu\Delta_{c\nu} + \Omega_{\rm baryon}\Delta_{c,\rm baryon}$). We define our transfer function as

$$T(k) = \frac{\Delta(k,t_0)}{\Delta(k,t_i)} \frac{\Delta(k=0,t_i)}{\Delta(k=0,t_0)} , \qquad \text{(A1)}$$

where t_i and t_0 are the initial and present times, respectively. The transfer functions are accurate to a few percent down to $k = 1h/\ {\rm Mpc}^{-1}$.

$$T(k) = \frac{1}{1 + t_1 k^{0.5} + t_2 k^1 + t_3 k^{1.5} + t_4 k^2 + t_5 k^{2.5}} . \qquad \text{(A2)}$$

In Table II, all coefficients are for k in Mpc (with h=0.5).

APPENDIX B: ESTIMATING THE CONTRIBUTION OF NONLINEAR EFFECTS

In the preceding section we alluded to the fact that nonlinear effects were becoming important at $8h^{-1}$ Mpc. We would like to estimate the size of the nonlinear effects.

To get a crude estimate we use the "spherical collapse model" treatment (see, e.g., Ref. [75]). This approximates a spherical overdensity in a flat universe locally as a miniature closed collapsing universe, so one can follow the collapse into the nonlinear regime. We can define the nonlinear overdensity as $\sigma^{\rm nonlin}$, which is given by the following equation:

$$\sigma^{\rm nonlin} = \frac{\rho}{\rho_b} - 1 = \frac{9}{2}\frac{(\theta - \sin\theta)^2}{(1-\cos\theta)^3} - 1, \qquad \text{(B1)}$$

where ρ_b is the background density and θ is the conformal time coordinate, which parametrizes a closed space-time. For the same value of θ the linear theory predicts $\sigma^{\rm (lin)}$

$$\sigma^{\rm (lin)} = \frac{3}{20}[6(\theta - \sin\theta)]^{2/3} \ . \qquad \text{(B2)}$$

Thus if $\sigma^{\rm (nonlin)} = 0.6$, we can estimate $\sigma^{\rm (lin)} = 0.4$, a 50% correction. To keep within a range where the perturbations are linear we must restrict ourselves to scales where $\sigma^{\rm (nonlin)} \leq 0.4$, where nonlinear corrections are estimated to be $\leq 30\%$.

[1] A. Linde, *Particle Physics and Inflationary Cosmology* (Harwood Academic, New York, 1990); E. Kolb and M. Turner, *The Early Universe* (Addison-Wesley, New York, 1989).
[2] Q. Shafi and F. W. Stecker, Phys. Rev. Lett. **53**, 1292 (1984).
[3] R. K. Schaefer, Q. Shafi, and F. W. Stecker, Astrophys. J. **347**, 575 (1989).
[4] J. Holtzman, Astrophys. J. Suppl. **74**, 1 (1989).
[5] F. Occhionero and R. Scaramella, Astron. Astrophys. **204**, 3 (1988).
[6] A. van Dalen and R. K. Schaefer, Astrophys. J. **398**, 33 (1992).
[7] J. A. Holtzman and J. R. Primack, Astrophys. J. **405**, 428 (1993); Y. P. Jing, H. J. Mo, G. Börner, and L. Z. Fang, *ibid.* **411**, 450 (1993).
[8] G. F. Smoot *et al.*, Astrophys. J. Lett. **396**, L1 (1992); E. L. Wright *et al.*, *ibid.* **396**, L13 (1992).
[9] R. K. Schaefer and Q. Shafi, Nature (London) **359**, 199 (1992).
[10] R. K. Schaefer and Q. Shafi, Phys. Rev. D **47**, 1333 (1993).
[11] M. G. Haehnelt, Mon. Not. R. Astron. Soc. **265**, 727 (1993); A. Nusser and J. Silk, Astrophys. J. Lett. **411**, L1 (1993).
[12] M. Davis, F. J. Summers, and D. Schlegel, Nature (London) **359**, 393 (1992).
[13] A. Klypin, J. Holtzman, J. Primack, and E. Regos, Astrophys. J. **416**, 1 (1993).
[14] Y. P. Jing, H. J. Mo, G. Börner, and L. Z. Fang, Astron. Astrophys. (to be published).
[15] G. Efstathiou, J. R. Bond, and S. D. M. White, Mon. Not. R. Astron. Soc. **258**, 1P (1992).
[16] D. Schlegel, M. Davis, F. Summers, and J. A. Holtzman, UCB report, 1993 (unpublished).
[17] S. Xiang and T. Kiang, Mon. Not. R. Astron. Soc. **259**, 761 (1992).
[18] A. N. Taylor and M. Rowan-Robinson, Nature (London) **359**, 396 (1992).
[19] D. Yu. Pogosyan and A. A. Starobinski, Mon. Not. R. Astron. Soc. **265**, 507 (1993).
[20] Q. Shafi and C. Wetterich, Phys. Lett. **129B**, 387 (1983); **152B**, 51 (1985); F. Lucchin, S. Matarrese, and S. Mollerach, Astrophys. J. Lett. **401**, L49 (1992).
[21] T. P. Walker, G. Steigman, D. N. Schramm, K. A. Olive, and H.-S. Kang, Astrophys. J. **376**, 51 (1991); M. S. Smith, L. H. Kawano, and R. A. Malaney, Astrophys. J. Suppl. **85**, 219 (1993).
[22] A. Dekel, E. Bertschinger, A. Yahil, M. A. Strauss, M. Davis, and J. P. Huchra, Astrophys. J. **412**, 1 (1993).
[23] J. N. Bahcall *et al.*, Astrophys. J. **387**, 56 (1992); D. Maoz *et al.*, *ibid.* **402**, 69 (1993); D. Maoz and H.-W. Rix, *ibid.* (to be published).
[24] A. R. Liddle and D. H. Lyth, Phys. Rep. **231**, 1 (1993).
[25] E. L. Wright *et al.*, Astrophys. J. **420**, 1 (1994).
[26] K. Ganga, E. Cheng, S. Meyer, and L. Page, Astrophys. J. Lett. **410**, L57 (1993).
[27] G. Efstathiou, N. Kaiser, W. Saunders, A. Lawrence, M. Rowan-Robinson, R. S. Ellis, and C. S. Frenk, Mon. Not. R. Astron. Soc. **247**, 10P (1990).
[28] K. B. Fisher, M. Davis, M. A. Strauss, A. Yahil, and J. P. Huchra, Astrophys. J. **389**, 188 (1992).
[29] H. Feldman, N. Kaiser, and J. A. Peacock, University Michigan Report No. UM AC 93-5 (unpublished).
[30] A. Dekel, in Observational Cosmology, Milan, 1992, edited by G. Chincarini *et al.*, A.S.P. Conf. No. 51 (unpublished).
[31] Y. Avni, Astrophys. J. **210**, 642 (1976).
[32] L. F. Abbott and M. Wise, Phys. Lett. **135B**, 279 (1984).
[33] L. F. Abbott and R. K. Schaefer, Astrophys. J. **308**, 546 (1986).
[34] R. Crittenden, J. R. Bond, R. L. Davis, G. Efstathiou, and P. J. Steinhardt, Phys. Rev. Lett. **71**, 324 (1993).
[35] M. Turner, Phys. Rev. D **48**, 3502 (1993).
[36] L. F. Abbott and M. Wise, Nucl. Phys. **B244**, 541 (1984).
[37] T. Souradeep and V. Sahni, IUCAA report, 1992 (unpublished).
[38] N. Kaiser, Mon. Not. R. Astron. Soc. **227**, 1 (1987).
[39] J. A. Peacock, Mon. Not. R. Astron. Soc. **259**, 494 (1992).
[40] N. Kaiser, G. Efstathiou, R. Ellis, C. S. Frenk, A. Lawrence, M. Rowan-Robinson, and W. Saunders, Mon. Not. R. Astron. Soc. **252**, 1 (1991).
[41] M. Rowan-Robinson, W. Saunders, A. Lawrence, and K. L. Leech, Mon. Not. R. Astron. Soc. **253**, 485 (1991).
[42] G. Efstathiou and M. J. Rees, Mon. Not. R. Astron. Soc. **230**, 5 (1988).
[43] M. G. Haehnelt and M. J. Rees, Mon. Not. R. Astron. Soc. **263**, 168 (1993).
[44] S. D. M. White, G. Efstathiou, and C. S. Frenk, Mon. Not. R. Astron. Soc. **262**, 1023 (1993).
[45] W. Saunders, M. Rowan-Robinson, and A. Lawrence, Mon. Not. R. Astron. Soc. **258**, 134 (1992).
[46] K. B. Fisher, M. Davis, M. A. Strauss, A. Yahil, and J. P. Huchra, Mon. Not. R. Astron. Soc. **266**, 50 (1994).
[47] M. Davis, G. Efstathiou, C. S. Frenk, and S. D. M. White, Astrophys. J. **292**, 371 (1985).
[48] H. M. P. Couchman and R. G. Carlberg, Astrophys. J.

389, 453 (1992).
[49] J. Gelb and E. Bertschinger, Astrophys. J. (to be published).
[50] J. Gelb, B.-A. Gradwohl, and J. Frieman, Astrophys. J. Lett. **403**, L5 (1993).
[51] J. M. Bardeen, J. R. Bond, N. Kaiser, and A. S. Szalay, Astrophys. J. **304**, 15 (1986).
[52] W. H. Press and P. Schecter, Astrophys. J. **187**, 425 (1974).
[53] E. Bertschinger and B. Jain, MIT Report No. MIT-CSR-93-12, 1993 (unpublished).
[54] C. S. Frenk, S. D. M. White, G. Efstathiou, and M. Davis, Astrophys. J. **351**, 10 (1990).
[55] J. G. Bartlett and J. Silk, Astrophys. J. Lett. **407**, L45 (1993).
[56] A. R. Liddle and D. H. Lyth, Mon. Not. R. Astron. Soc. **265**, 369 (1993).
[57] R. Holman, G. Lazarides, and Q. Shafi, Phys. Rev. D **27**, 995 (1983); Q. Shafi, in *Europhysics Conference on Electroweak Effects, Erice, 1983*, edited by Harvey B. Newman (Plenum, New York, 1985); R. N. Mohapatra and G. Senjanovic, Z. Phys. C **17**, 53 (1983).
[58] N. G. Deshpande, E. Keith, and P. B. Pal, Phys. Rev. D **46**, 2261 (1992).
[59] M. Gell-Mann, P. Ramond, and R. Slansky, in *Supergravity*, edited by P. van Nieuwenhuizen and D. Freedman (North-Holland, Amsterdam, 1979); T. Yanagida (unpublished).
[60] For recent analyses, see *Neutrino '92*, Proceedings of the XVth International Conference on Neutrino Physics and Astrophysics, Granada, Spain, edited by A. Morales [Nucl. Phys. B (Proc. Suppl.) **31**, 1 (1993)].
[61] R. Peccei and H. Quinn, Phys. Rev. Lett. **38**, 1440 (1977); S. Weinberg, *ibid.* **40**, 223 (1978); F. Wilczek, *ibid.* **40**, 279 (1978).
[62] Q. Shafi and A. Vilenkin, Phys. Rev. Lett. **52**, 691 (1984); G. Lazarides and Q. Shafi, Phys. Lett. **148B**, 35 (1984).
[63] G. Lazarides and Q. Shafi, Phys. Lett. B **258**, 305 (1991); G. Lazarides, C. Panagiotokopoulos, and Q. Shafi, *ibid.* **315**, 325 (1993); M. Fukugita and T. Yanagida, Phys. Lett. B **174**, 45 (1986).
[64] J. Harvey and M. Turner, Phys. Rev. D **42**, 3344 (1990).
[65] S. Y. Pi, Phys. Rev. Lett. **52**, 1725 (1984).
[66] U. Amaldi, W. de Boer, and H. Fürstenau, Phys. Lett. B **260**, 447 (1991); J. Ellis, S. Kelley, and D. V. Nanopoulos, *ibid.* **249**, 441 (1990); P. Langacker and M. Luo, Phys. Rev. D **44**, 817 (1991).
[67] T. W. B. Kibble, G. Lazarides, and Q. Shafi, Phys. Lett. **113B**, 237 (1982); S. P. Martin, Phys. Rev. D **46**, 2769 (1992).
[68] B. Ananthanarayan, G. Lazarides, and Q. Shafi, Phys. Rev. D **44**, 1613 (1991); Phys. Lett. B **300**, 245 (1993).
[69] G. Lazarides and Q. Shafi, Nucl. Phys. **B350**, 179 (1991); K. Babu and Q. Shafi, Phys. Rev. D **47**, 5004 (1993); G. Anderson *et al.*, *ibid.* **49**, 3660 (1994), and references therein.
[70] G. Lazarides and Q. Shafi, Phys. Lett. B **308**, 17 (1993).
[71] P. Candelas, G. Horowitz, A. Strominger, and E. Witten, Nucl. Phys. **B258**, 46 (1985); E. Witten, *ibid.* **B258**, 75 (1985).
[72] D. Gross, J. Harvey, E. Martinez, and R. Rohm, Phys. Rev. Lett. **56**, 502 (1985).
[73] H. Kodama and M. Sasaki, Prog. Theor. Phys. Suppl. **74**, 1 (1984).
[74] R. K. Schaefer, Int. J. Mod. Phys. A **6**, 2075 (1991).
[75] P. J. E. Peebles, *The Large Scale Structure of the Universe* (Princeton University Press, Princeton, NJ, 1980).